Available online at www.sciencedirect.com

ScienceDirect

Procedia Structural Integrity 33 (2021) 578–585

Structural Integrity Procedia

www.elsevier.com/locate/procedia

IGF26 - 26th International Conference on Fracture and Structural Integrity

Quasi-static behavior of 3D printed lattice structures of various scales

Zhuo Xu[a], Elena Medori[a,b], Fabrizio Sarasini[b], Seyed Mohammad Javad Razavi[a*]

[a]*Department of Mechanical and Industrial Engineering, Norwegian University of Science and Technology, Richard Birkeland vei 2B, 7491, Trondheim, Norway*

[b]*Department of Chemical Engineering Materials Environment, Sapienza University of Rome, Via Eudossiana 18, 00184 Roma (RM), Italy*

Abstract

Additive manufacturing technology has been playing an important role in industrial applications due to the potential capacities to fabricate complex geometries such as lattice structures, which are treated as outstanding candidates for biomedical implants, lightweight energy absorption, and heat dissipation applications from relatively small to large scale. According to the recent research studies in the literature, the mechanical properties of conventionally designed parts fabricated via additive manufacturing are highly dependent on the size and thickness of the parts. The significance of the scale effect on more complex designs such as lattice structures has not been yet fully investigated for polymeric structures. Therefore, this study aims to investigate the scale and wall thickness effect on the mechanical properties of various uniform lattice structures. First, cubic test specimens are designed and divided into two categories with the dimensional constraints of keeping the constant porosity and cubic size in each category. Then a variety of sheet periodic minimal surface (TPMS) based gyroid lattices are fabricated with PLA (Polylactic Acid) via the FDM technique. The manufactured specimens are then subjected to compressive loading to evaluate the mechanical strength and the energy absorption per unit volume. High-resolution images are captured in order to monitor the failure mechanism during the tests. Finally, the experimental results from compression tests are compared and the systematic dependence of the mechanical behavior on the scale and wall thickness effect is discussed.

© 2021 The Authors. Published by Elsevier B.V.
This is an open access article under the CC BY-NC-ND license (https://creativecommons.org/licenses/by-nc-nd/4.0)
Peer-review under responsibility of the scientific committee of the IGF ExCo

* Corresponding author.
E-mail address: javad.razavi@ntnu.no

2452-3216 © 2021 The Authors. Published by Elsevier B.V.
This is an open access article under the CC BY-NC-ND license (https://creativecommons.org/licenses/by-nc-nd/4.0)
Peer-review under responsibility of the scientific committee of the IGF ExCo
10.1016/j.prostr.2021.10.064

Keywords: Fused deposition modelling (FDM); TPMS lattice; Thickness & scale effect; PLA; Additive Manufacturing; Compression tests

1. Introduction

Additive manufacturing (AM) methods enable the fabrication of components with fully customizable shapes and mechanical characteristics, which cannot be manufactured by conventional manufacturing techniques like CNC (Brandt et al. 2013). It is a revolutionary technology for directly fabricating components from a digital CAD model utilizing a layer-by-layer material build-up process. This toolless manufacturing technology is capable of producing highly dense parts in a short amount of time with a high degree of accuracy. Moreover, it has the capability of fabricating components with complex geometries such as lattice structures, which have been widely adopted in the field of biomedical implants (Wang et al. 2018),(Kladovasilakis, Tsongas, and Tzetzis 2020),(Moiduddin et al. 2020),(Murr et al. 2012), heat dissipation applications (Wadley and Queheillalt 2007), light-weighting of aerospace components (Zhu, Li, and Childs 2018), and energy absorption for personal protective equipment (Brennan-Craddock et al. 2012).

Fused deposition modeling (FDM) or fused filament fabrication (FFF) is a well-reputed one of the material extrusion AM technology. A thermoplastic filament is heated to a certain temperature and extruded through a nozzle, then the molten material from the print head is deposited on the surface of the building platform to create the 3D structures. The movement of the nozzle and building plate is controlled by the G-code files generated by the slicing software containing pre-defined printing process parameters. It is capable of fabricating components with material complexities and unprecedented geometry, such as functionally graded materials and various lattice structures.

Lattice structures are porous structures composed of a periodic arrangement of three-dimensional (3D) unit cells with a pre-determined volume fraction ratio. Volume fraction can also be referred to as relative density, which is one of the critical parameters for controlling and manipulating lattice structures with varying gradients. In general, lattices can be classified into three types including strut-based lattices, solid-TPMS based lattices, and sheet-TPMS based lattices, where triply periodic minimal surface (TPMS) is a minimal surface that sometimes can be referred to as implicit-based unit cells (Al‐Ketan and Abu Al‐Rub 2020),(Benedetti et al. 2021).

The minimal surface can be defined and characterized by mean curvature of zero at any point (Al‐Ketan and Abu Al‐Rub 2020). These surfaces exhibit both remarkable and unique properties. For instance, a minimal surface does not consist of any sharp edges or corners in nature. According to the literature review, the level-set approximation approach is the simplest and most extensively used technique to model 3D lattices. The level-set method (LSM) is a methodological framework that is mostly used to analyze surfaces and shapes numerically. The level-set function can be defined as $\emptyset(x,y,z) = c$ where $\emptyset$ is an evaluated iso-surface while c is an iso-value. For instance, the level-set equation for gyroid structures is listed below (Al‐Ketan and Abu Al‐Rub 2020):

$$\sin X \cos Y + \sin Y \cos Z + \sin Z \cos X = c \tag{1}$$

where $X = 2\alpha\pi x,\ Y = 2\beta\pi y, Z = 2\gamma\pi z.\ \alpha, \beta,$ and γ are all constants corresponding to the unit cell size in the x, y and z directions, respectively.

One of the widely used architectural shapes for biomedical applications is solid or sheet-TPMS based gyroid lattices discovered by Schoen in 1970. Since then, researchers have continuously demonstrated that gyroid architecture is suitable for biomorphic scaffold design in tissue engineering because of its outstanding mechanical properties. Particularly, (Kapfer et al. 2011) reported that the sheet-based gyroid lattice structures have higher stiffness than the solid-based gyroid structure at the same porosity of the same material. Similarly, (Al-Ketan, Rowshan, and Abu Al-Rub 2018) investigated the mechanical properties of a wide range of structures, including strut-based, solid-based TPMS, and sheet-based TPMS porous structures. The experimental results revealed that the sheet-based TPMS structure has superior mechanical properties in terms of stress-strain responses. Although numerous researchers have already investigated the compression behaviors of various sheet-based TPMS lattice structures fabricated via different AM processes and materials. However, there is a lack of research on the size and wall thickness influence of mechanical properties for FDM fabricated specimens.

Nomenclature

AM	additive manufacturing
CAD	computer-aided design
CNC	computer numerical control
DIC	digital image correlation
FDM	fused deposition modeling
FFF	fused filament fabrication
PLA	polylactic acid
TPMS	Triply periodic minimal surfaces
UTS	ultimate tensile strength

2. Experimental procedures

2.1. Design and fabrication process

This research aims to investigate the scale and wall thickness effect on the mechanical properties of various uniform lattice structures. Specifically, sheet-TPMS based gyroid lattice structures were selected in this project. Geometry parameters of lattices such as cube size, unit cell size, wall thickness, and porosity, were determined and divided into two categories, including scale effect at constant porosity and wall thickness effect at constant cube size and unit cell size. Detailed geometries and parameters are illustrated in Tables 1 and 2. In addition, lattice names corresponding to their geometrical dimensions are presented in Table 3. For instance, G stands for gyroid, the following number represents the unit cell size while the other represents wall thickness.

All the lattices were fabricated via FDM technique by using an Original Prusa i3 MK3 with a filament diameter of 1.75mm. Black PLA filament manufactured by 3DNet was selected as a feedstock for the purpose of better DIC analysis due to the better contrast color of speckle and spray. All lattice models were imported into a slicing software Ultimaker Cura 4.8.0 in order to generate G-codes with pre-defined printing process parameters such as printing speed, extrusion & building platform temperature, and raster angles. In addition, all the lattices were fabricated with 100% infill density in order to approach as closely as possible for the optimal mechanical properties of fully dense material (Torres et al. 2016). Moreover, the raster angles were determined to be ± 45 degrees for alternative layers. All detailed essential process parameters are listed in Table 4. These process parameters were determined based on the fabrication quality of lattices, especially for the ones with the smallest unit cell and cubic size, which required additional tuning on filament retractions speed and distance while printing between lines to avoid potential stringing or oozing issues (Kumar, Verma, and Jeng 2020).

Table 1: 1st category - Scale effect at constant porosity of 68.72%

Lattice name	G-4-0.645	G-8-1.29	G-12-1.935
Cube size (mm)	16	32	48
Unit cell size (mm)	4	8	12
Wall thickness (mm)	0.645	1.29	1.935
Porosity (%)	68.72%	68.72%	68.72%

Table 2: 2nd category - wall thickness effect at constant cube size of 32mm and unit cell size of 8mm

Lattice name	G-8-0.645	G-8-1.29	G-8-1.935
Cube size (mm)	32	32	32
Unit cell size (mm)	8	8	8
Wall thickness (mm)	0.645	1.29	1.935
Porosity (%)	84.38%	68.72%	57.75%

Table 3: Lattice naming rules and dimensions

Name	Overall Cell size (mm)	Unit cell size (mm)	Wall thickness (mm)
G-4-0.645	16x16x16	4	0.645
G-8-0.645	32x32x32	8	0.645
G-8-1.29	32x32x32	8	1.29
G-8-1.935	32x32x32	8	1.935
G-12-1.935	48x48x48	12	1.935

Table 4: Process parameters used for fabricating the lattice structures.

Building parameters	Parameter value	Building parameters	Parameter value	Building parameters	Parameter value
Layer height	0.15mm	Build plate temperature	75 °C	Infill density	100%
Infill line distance	0.4mm	Printing speed	50mm/s	Raster angles	±45 degrees
Wall thickness	0.8mm	Initial layer printing speed	40mm/s	Retraction speed	35mm/s
Wall line count	2	Retraction distance	0.5mm	Nozzle temperature	215 °C

2.2. Quasi-static compression tests

A servo-hydraulic MTS 809 multi-axial machine with a load cell of 100 kN (Fig.1) was used for compression tests of the fabricated lattices to investigate the failure mechanism and stress-strain response experimentally. Specimens were placed between two plates where the lower plate is stationary during the compression tests. In order to eliminate the other potential discrepancies and maintain consistent results, the same orientation of lattices was used when placing the lattices on the compression plate compared to the printing orientation. No lubricant was used on the contact surfaces between lattices and plates. The compression rate was set to be 2mm/min and the sampling rate of 20Hz. The ultimate compression strain was set to be approximately 50% of the original height. A fixed camera system was also used to capture high-resolution images with a predefined sampling frequency during the compression tests.

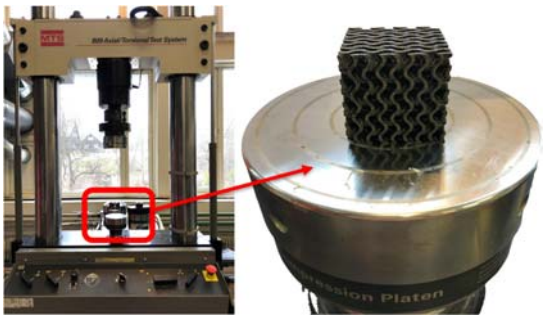

Fig. 1. MTS 809 testing machine and compression plate

3. Results and Discussions

Compression load and displacement data were recorded during the tests and then computed to obtain the stress and engineering strain data. The results were classified into two categories corresponding to scale effect at constant porosity and wall thickness effect at the constant cubic size. The dimensions of each lattice were measured with a caliper in order to obtain more accurate computational results of stress and strain. Stress was calculated based on the formula that compression load divided by the effective area of contacting surface. In this case, the effective area can be calculated with the actual dimensions of the lattice multiplied by the percentage of relative density because of the uniformity of the lattice. While strain was calculated based on the actual compression displacement divided by the original height of the lattice. In addition, cumulative energy absorption per unit volume was calculated based on the area under the stress-strain curve.

Fig. 2.a illustrates the stress-strain characteristic of scale effect under constant porosity. In this category, a porosity of 68.72% was selected for this study because it is a typical specification for structures that are suitable for biomedical applications in orthopedic surgery (Mullen et al. 2009). The experimental results revealed that all the stress-strain curves demonstrated a similar trend with only one peak and valley. The peak stress occurred approximately at 5% of the strain while the densification strain occurred between 20-30% of the strain. In addition, all the curves have the tendency to merge into one point when approaching 50% of the strain. It also can be observed that the maximum stress increases when the unit cell size and wall thickness increase. Similar trends and characteristics can also be observed for the stress-strain curve of wall thickness effect under constant cubic and unit cell size as illustrated in Fig. 2.b. It was discovered that the lattice structures with the thickest and thinnest wall thickness have the largest and smallest peak compressive strength, respectively. The porosity of the lattice structures decreases when the wall thickness increases. Besides, it was also noticeable the lattice structures with relatively larger wall thickness (G-8-1.29 & G-8-1.935) experience only one peak and valley on the stress-strain curve, while the lattice with relatively smaller wall thickness (G-8-0.645) experiences multiple peaks and valleys during the plateau region. These experimental results indicated that two different failure mechanisms occurred for those lattice structures during the compression tests, including layer successive collapse (as illustrated in Fig. 3.a) and globally uniform deformation (as illustrated in Fig. 3.b and 3.c). As for the layer successive collapse mechanism particularly, the strain started to localize beyond the elastic region with consecutive layer-by-layer failure and the number of peaks and valleys of the corresponding stress-strain curve directly relates to the number of layers in the direction of compression.

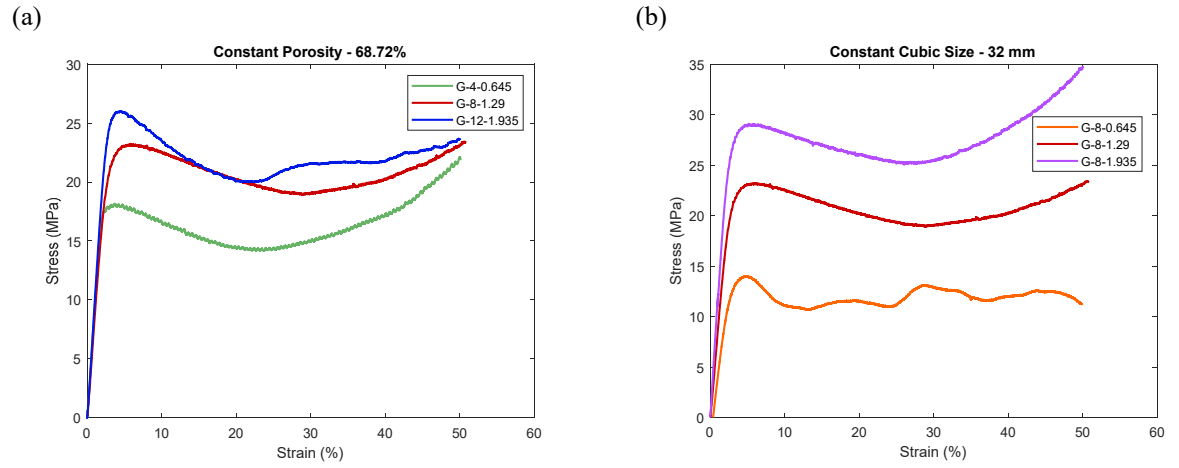

Fig.2. (a) Stress versus strain curves of scale effect under constant porosity, (b) Stress versus strain curves of wall thickness effect under constant cubic size and unit cell size

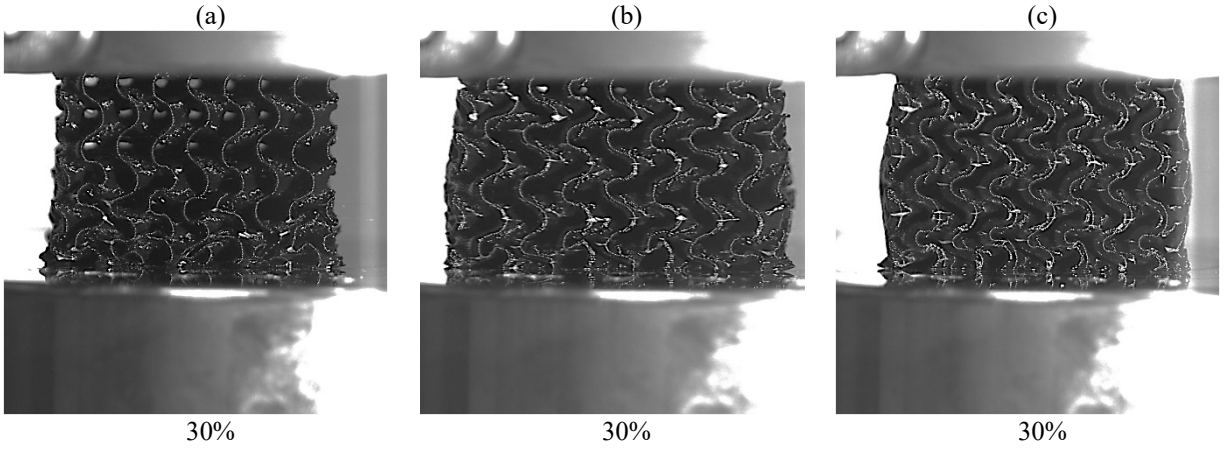

Fig. 2. (a) Image from the compression of lattice G-8-0.645 fabricated via FDM process with PLA under 30% strain, (b) Image from the compression of lattice G-8-1.29 fabricated via FDM process with PLA under 30% strain, (c) Image from the compression of lattice G-8-1.935 fabricated via FDM process with PLA under 30% strain.

Cumulative energy absorption per unit volume versus strain of scale effect under constant porosity is illustrated in Fig. 4.a. The results indicate that lattices with the smallest/largest unit cells and wall thickness (G-4-0.645 and G-12-1.935) have the smallest/largest energy absorption per unit volume, respectively. The differences between G-12-1.935 and G-8-1.29 are significantly smaller than those between G-8-1.29 and G-4-0.645. One possible reason is that defects such as voids and stringing are more likely to occur for lattices with both smaller unit cell sizes and smaller wall thicknesses during the fabrication, which can result in relatively lower accumulative energy absorption per unit volume. In addition, all three curves of energy absorption per unit volume demonstrate an almost linear trend within the 0-50% of the strain, which indicates the densification strain will occur after 50% (Maskery et al. 2016). A similar trend was observed for the cumulative energy absorption curves of wall thickness effect under constant cubic and unit cell size in Fig. 4.b as well. It was discovered that the lattice structures with the thickest and thinnest wall thickness have the largest and smallest energy absorption per unit volume under the same strain value,

respectively. Besides, similar to the curves in Fig. 4.a, all the curves exhibit almost linear trends within 0-50% of the strain.

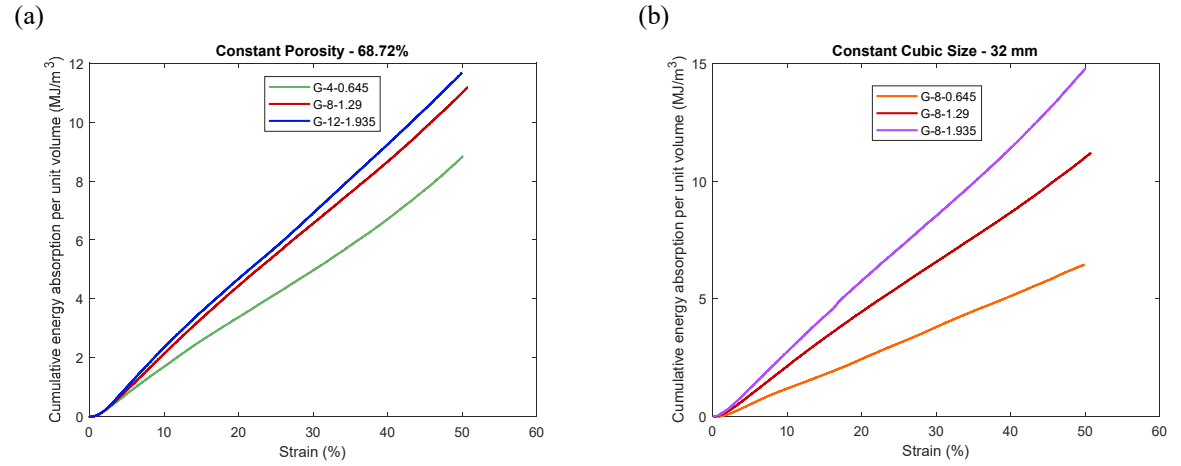

Fig. 4. (a) Cumulative energy absorption per unit volume versus strain of scale effect under constant porosity, (b) Cumulative energy absorption per unit volume versus strain of wall thickness effect under constant cubic size and unit cell size

4. Conclusion

Overall, the scale and wall thickness effect on the mechanical properties of various uniform sheet-TPMS based lattice structures fabricated via FDM technology with PLA were investigated in this study. Two categories corresponding to scale effect at constant porosity and wall thickness effect at constant cubic and unit cell size were considered for comparisons in terms of mechanical behavior.

The experimental results indicate that there is a high degree of association between various scales of lattice structures and their related mechanical behavior. The same phenomenon was observed for the lattice structures with different wall thicknesses as well. Specifically, lattices with both larger scale and larger wall thickness experience higher ultimate compressive strength according to the stress-strain curves. One of the reasons is that increased wall thickness results in an increase in relative density, which leads to higher peak compressive strength and larger energy absorption. In addition, except for one curve, all other stress-strain curves have similar trends with only one peak and valley, which indicate a globally uniform failure mechanism during the compression tests. On the contrary, the unique lattice structure displayed distinctive features with multiple peaks and valleys due to the possible buckling and folding of the cell walls along with the compression as described earlier. Besides, all the curves reached the ultimate compressive strength at nearly the same strain (5%) regardless of the wall thickness and scale. Furthermore, as for the energy absorption performance, larger scale and wall thickness will increase the cumulative energy absorption per unit volume under the same strain value.

5. References

Al-Ketan, Oraib, Reza Rowshan, and Rashid K. Abu Al-Rub. 2018. “Topology-Mechanical Property Relationship of 3D Printed Strut, Skeletal, and Sheet Based Periodic Metallic Cellular Materials.” *Additive Manufacturing* 19(January): 167–83.

Al-Ketan, Oraib, and Rashid K. Abu Al-Rub. 2020. “MSLattice: A Free Software for Generating Uniform and Graded Lattices Based on Triply Periodic Minimal Surfaces.” *Material Design & Processing Communications*: 0–3.

Benedetti, M. et al. 2021. “Architected Cellular Materials: A Review on Their Mechanical Properties towards Fatigue-Tolerant Design and Fabrication.” *Materials Science and Engineering R: Reports* 144: 100606. https://doi.org/10.1016/j.mser.2021.100606.

Brandt, M. et al. 2013. “High-Value SLM Aerospace Components: From Design to Manufacture.” *Advanced Materials Research* 633(January):

135–47.
Brennan-Craddock, J., D. Brackett, R. Wildman, and R. Hague. 2012. "The Design of Impact Absorbing Structures for Additive Manufacture." *Journal of Physics: Conference Series* 382(1).
Kapfer, Sebastian C. et al. 2011. "Minimal Surface Scaffold Designs for Tissue Engineering." *Biomaterials* 32(29): 6875–82. http://dx.doi.org/10.1016/j.biomaterials.2011.06.012.
Kladovasilakis, Nikolaos, Konstantinos Tsongas, and Dimitrios Tzetzis. 2020. "Finite Element Analysis of Orthopedic Hip Implant with Functionally Graded Bioinspired Lattice Structures." *Biomimetics* 5(3).
Kumar, Ajeet, Saurav Verma, and Jeng Ywan Jeng. 2020. "Supportless Lattice Structures for Energy Absorption Fabricated by Fused Deposition Modeling." *3D Printing and Additive Manufacturing* 7(2): 85–96.
Maskery, I. et al. 2016. "A Mechanical Property Evaluation of Graded Density Al-Si10-Mg Lattice Structures Manufactured by Selective Laser Melting." *Materials Science and Engineering A* 670: 264–74. http://dx.doi.org/10.1016/j.msea.2016.06.013.
Moiduddin, Khaja et al. 2020. "Integrative and Multi-Disciplinary Framework for the 3D Rehabilitation of Large Mandibular Defects." *International Journal of Advanced Manufacturing Technology* 106(9–10): 3831–47.
Mullen, Lewis et al. 2009. "Selective Laser Melting: A Regular Unit Cell Approach for the Manufacture of Porous, Titanium, Bone in-Growth Constructs, Suitable for Orthopedic Applications." *Journal of Biomedical Materials Research - Part B Applied Biomaterials* 89(2): 325–34.
Murr, Lawrence E. et al. 2012. "Next Generation Orthopaedic Implants by Additive Manufacturing Using Electron Beam Melting." *International Journal of Biomaterials* 2012.
Torres, Jonathan et al. 2016. "An Approach for Mechanical Property Optimization of Fused Deposition Modeling with Polylactic Acid via Design of Experiments." *Rapid Prototyping Journal* 22(2): 387–404.
Wadley, Haydn N.G., and Douglas T. Queheillalt. 2007. "Applications of Cellular Lattice Structures." *Materials Science Forum* 539–543: 242–47.
Wang, Yingjun, Sajad Arabnejad, Michael Tanzer, and Damiano Pasini. 2018. "Hip Implant Design with Three-Dimensional Porous Architecture of Optimized Graded Density." *Journal of Mechanical Design, Transactions of the ASME* 140(11): 1–13.
Zhu, L., N. Li, and P. R.N. Childs. 2018. "Light-Weighting in Aerospace Component and System Design." *Propulsion and Power Research* 7(2): 103–19.